FISEVIER

Contents lists available at ScienceDirect

# **Chemical Physics Impact**

journal homepage: www.sciencedirect.com/journal/chemical-physics-impact



Full Length Article

# Pisolithus Arhizus dye: A novel natural dopant for tailoring nonlinear optical properties of guanidinium carbonate single crystals

K. Divya<sup>a</sup>, Amutha Soosairaj<sup>a</sup>, A. Alex Arunmozhi<sup>a</sup>, A. Leo Rajesh<sup>b,\*</sup>

- a Department of Physics, St. Joseph's College (Autonomous), Affiliated to Bharathidasan University, Tiruchirappalli 620002, Tamil Nadu, India
- <sup>b</sup> Department of Physics, School of Physical, Chemical and Applied Sciences, Pondicherry University, Pondicherry 605014, India

#### ARTICLE INFO

Keywords:
Natural dye-doped single crystals
Optical properties
Thermal stability
Mechanical properties
SHG efficiency

#### ABSTRACT

In the realm of crystal growth, the utilization of dopant materials plays a pivotal role in tailoring the properties of single crystals. This research explores the incorporation of natural dyes, specifically the pigment derived from the Pisolithus Arhizus fungus extract, as a dopant material in the growth process of Guanidinium Carbonate (GC) single crystals. Comparative analyses were carried out between the dye-doped crystals and their undoped counterparts, revealing significant enhancements in the growth period, optical properties, mechanical properties, thermal properties and second harmonic generation (SHG) efficiency of the dye-doped crystals. Structural characterizations, including single crystal and powder X-ray diffraction techniques, confirmed the crystalline nature of both undoped and dye-doped crystals. Fourier Transform Infrared (FTIR) analysis validated the existence of functional groups, while Energy Dispersive X-ray Analysis (EDAX) confirmed the presence of dye molecules within the crystal lattice. UV-Visible spectroscopy and microhardness studies revealed enhanced optical and mechanical characteristics in dye-doped crystals compared to undoped ones. Thermogravimetric and Differential Thermal analysis (TG-DTA) indicate improved thermal stability in dye-doped crystals. The non-linear optical characterization showed 1.73 times increase in SHG efficiency in dye-doped crystals compared to undoped GC crystals. Therefore, including dye molecules in the crystal lattice improved the optical, thermal, mechanical properties and SHG efficiency, making dye-doped crystals suitable candidates for various optical applications.

# Introduction

Single crystals serve as fundamental components for the majority of solid-state devices and find significant applications in research and development across various fields, including electronics, photonics, fiber optics, and the semiconductor industry. Single crystals, particularly those with non-centrosymmetric arrangements of atoms or molecules, have been extensively studied as a nonlinear optical (NLO) materials due to their lack of grain boundaries and ability to achieve high crystalline perfection, making them applicable in nonlinear optical applications [1–3]. Organic materials attract considerable attention due to their substantial instantaneous nonlinear optical and electronic responses, including conductivity, susceptibility, high laser damage threshold, and structural flexibility compared to inorganic crystalline materials. These properties are owed to the presence of  $\pi$ -conjugated electron systems, making them suitable for a wide range of nonlinear optical applications [4].

The remarkable nonlinear optical characteristics of guanidine salts and derivatives arising from the presence of delocalized  $\pi$ -electrons and hydrogen-bonded networks have motivated an investigation into guanidine salts [5]. Guanidine, an extremely strong base, forms its ion through protonation. It readily interacts with high crystalline organics salts and is a water-soluble chemical with high alkalinity. Due to six possible donor sites for hydrogen-bonding interactions, the guanidinium cation can efficiently attach to various inorganic and organic anions, as well as polyanions [6,7]. Guanidinium finds applications in supramolecular recognition processes in chemical, biological and medicinal chemistry, with a specific emphasis on its potential uses in nonlinear optics [8-10]. In recent studies, researchers in crystal growth have described several guanidinium based nonlinear optical single crystals, including guanidinium isophthalate [4], guanidinium l-glutamate [5], guanidinium nitrate [11], barium guanidinium dichloride [8], guanidinium pentaborate monohydrate [12] and guanidinium chromate [13].

Additionally, researchers have shown an increasing interest in recent

E-mail address: aleorajesh@gmail.com (A. Leo Rajesh).

<sup>\*</sup> Corresponding author.

years in incorporating synthetic dyes into organic crystals for various optical applications in lasers and solid-state devices [14,15]. However, the majority of synthetic dye doped organic crystals undergo difficult synthesis and crystal growth procedures, exhibit poor thermal stability, weak mechanical hardness and are generally expensive, toxicity, non-biodegradable and hazardous [16] in nature. These challenges have prompted researchers to search for novel optical materials that are inexpensive, safe and possess enhanced nonlinear optical properties. Natural dyes derived from organic sources have long held appeal for their ecological sustainability and vibrant molecular structures, making them suitable for diverse applications [17]. The existing studies predominantly focus on synthetic dyes as dopants in organic nonlinear optical materials, with no attention given to natural dyes despite their potential advantages in terms of sustainability, biocompatibility and environmental friendliness. Therefore, this study aims to bridge this gap by exploring the incorporation of natural dyes into guanidinium carbonate single crystals for nonlinear optical applications to enhance the properties of the grown crystals. Further research into the unique integration of natural dyes could pave the way for more efficient and sustainable photonics technology.

Fungi constitute the second-largest category of organisms in the biosphere, with mushrooms playing a key role in forest ecosystems by thriving on the most prevalent biomolecules in the natural environment. Even though they have a universal and highly diverse nature, fungi, which are essential functional elements in forest ecosystems, have received less attention compared to animals and plants. One noteworthy fungus is *Pisolithus Arhizus* (Pers.), Rauschert [P. tinctorius (Mich. exPers.) Coker & Couch] is a Gasteromycetes fungus found globally. Additionally, it is commonly known as a dead man's foot, which exhibits an earth-ball-like appearance. Interestingly, the viscous gel derived from this puffball finds a practical application as a natural dye for clothing and it is consistently discovered in mycorrhizal association with various economically important tree genera [18–20].

In this study, high quality guanidinium carbonate (GC) single crystals were grown by slow evaporation technique. As a novel advancement, a natural dye extracted from the *Pisolithus Arhizus* fungus was utilized as a dopant for the first time to grow guanidinium carbonate single crystals. The undoped (GC) and *Pisolithus Arhizus* dye-doped (Fu-GC) guanidinium carbonate crystals were systematically characterized to elucidate modifications in structural, optical, thermal, mechanical and nonlinear properties arising from dye incorporation. Investigating the influence of the biosafe, eco-friendly Pisolithus dye on crystal growth and physicochemical attributes is aimed at evaluating its potential to enhance performance for diverse optical applications. The unique integration of a sustainably sourced natural fungal dye within guanidinium carbonate crystal lattice unlocks new possibilities for developing efficient nonlinear optical materials through green synthesis approaches.

#### **Experimental**

#### Sample collection

*Pisolithus Arhizus* fungi were freshly collected in the farm field in Killukottai, Pudukkottai district, Tamil Nadu, India at the following GPS co-ordinates: Site 1. Lat:  $10^\circ$  39′  $18'^\circ$  Long:  $78^\circ$  55′  $12'^\circ$ , Site 2. Lat:  $10^\circ$  39′  $18'^\circ$  Long:  $10^\circ$  39′  $10'^\circ$  Long:  $10^\circ$  39′  $10'^\circ$  Long:  $10^\circ$  39′  $10'^\circ$  Long:  $10^\circ$  55′  $10'^\circ$  10° 55′  $10'^\circ$ 

# Dye extraction from Pisolithus Arhizus fungus

The collected fungus was air dried under shade at room temperature for 24 h and ground into a fine powder using a mortar. The powdered samples were stored in dark, airtight containers at room temperature for further use. For the traditional solvent extraction method, 50~g of powdered samples were added to 100~mL of distilled water and kept for extraction for 24~h. After 24~h, the extracts were filtered using Whatmann filter paper, and the collected filtrates were stored refrigerator for further analysis.

### Solubility

The solubility of guanidinium carbonate was assessed in both water and methanol over a temperature range of 30–55  $^{\circ}$ C. The solution was consistently stirred and kept at a constant temperature to achieve a uniform concentration. After reaching saturation, the solution was observed gravimetrically and this procedure was repeated at regular intervals of 5  $^{\circ}$ C. Fig. 1 depicts the solubility curve of the undoped guanidinium carbonate crystal.

The solubility graph reveals a positive solubility trend in water, with a concentration of 12 g/100 ml observed at 30  $^{\circ}$ C. According to the solubility studies, water was identified as an optimal solvent for the growth of GC crystals. A supersaturated solution was prepared and allowed to slowly evaporate at 30  $^{\circ}$ C. The crystal quality was significantly enhanced by applying an effective recrystallization procedure.

#### Material synthesis

Commercially available Guanidine Carbonate (AR Grade, 99 %) was used as the raw material to synthesize the title compound. Guanidine carbonate was dissolved in double-distilled water and stirred for 2 h to achieve a homogeneous solution. The saturated solution was filtered using Whatman filter paper and kept for evaporation. Good-quality undoped guanidinium carbonate single crystals were obtained in a growth period of 37 days. The same procedure was followed to grow Pisolithus Arhizus dye-doped guanidinium carbonate single crystals, 0.05 % of the dye was added to the guanidine carbonate dissolved in double distilled water solution and stirred well to obtain a homogeneous mixture. After 2 h, the obtained solution was filtered and kept for evaporation. Stable, transparent, light-tinted Pisolithus Arhizus dyedoped Guanidinium Carbonate (Fu-GC) single crystals were obtained in a short growth period of 24 days. The incorporation of the dye affected the crystal growth period and kinetics in the GC crystals. Experimental results clearly indicated that the presence of the dye molecules led to a noticeable change in the nucleation process and reduced growth period as well. The as-grown crystals of undoped and dye-doped guanidinium carbonate are shown in Figs. 2a and 2b.

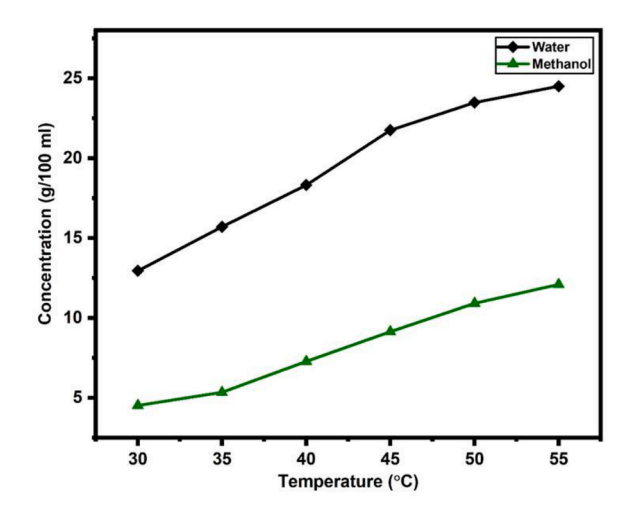


Fig. 1. Solubility curve of guanidinium carbonate.

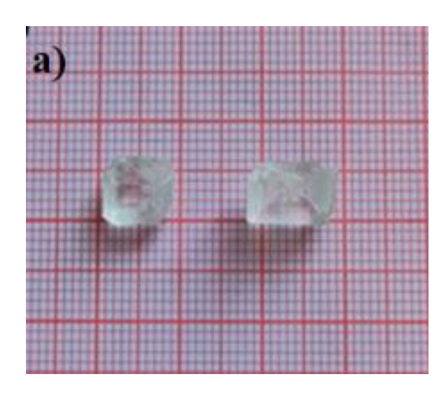




Fig. 2. Photograph of grown crystal. (a) Undoped Guanidinium Carbonate (b) Pisolithus Arhizus dye-doped Guanidinium Carbonate.

#### Results and discussion

Single crystal X-ray diffraction analysis

Single crystal X-ray diffraction (SCXRD) analysis was performed using a Mo K $\alpha$  ( $\lambda=0.71073$  Å) radiation source on a Brucker Q8 Quest diffractometer. The unit cell parameters, crystal system, and space group of the high-quality single crystals of GC and Fu-GC were determined through single crystal X-ray diffraction analysis. It was observed that both crystals crystallized in the non-centrosymmetric tetragonal system. The undoped crystal shows good agreement with the previously reported results [21]. The obtained cell parameters and cell volumes are listed in Table 1.

From the SCXRD analysis, dye doping didn't affect the crystal structure but there is a notable change in crystal morphology. A minor increase in lattice parameters can be attributed to lattice strain resulting from the incorporation of dye, leading to an expansion in cell volume.

# Powder X-ray diffraction analysis

The powder forms of undoped and dye-doped GC single crystals were utilized for powder X-ray diffraction analysis using an X'Pert Pro-Panalytical diffractometer with monochromatic Cu K $\alpha$  radiation ( $\lambda=1.5406$  Å). This analysis aimed to investigate the crystalline nature of the grown crystals. The corresponding data were obtained at room temperature, with diffraction angles ranging from  $10^\circ$  to  $70^\circ$  Fig. 3 displays the powder X-ray diffraction patterns of undoped and dye-doped GC samples. The (h k l) values were determined and indexed using the EXPO 2014 crystal structure solution software.

Analysis of the diffraction graph reveals well-defined Bragg peaks at specific  $2\theta$  values, indicating the high crystallinity of the grown crystals. However, changes in morphology have caused variations in the intensity of certain peaks, as a result of dye-doping.

#### UV-Visible analysis

The UV-Visible spectral analysis provides crucial structural insights,

**Table 1**Lattice Parameters obtained from single crystal X-ray diffraction.

Lattice Parameters	Undoped GC	Fu-GC
Crystal System	Tetragonal	Tetragonal
Space Group	$P \ 4_1 2_1 2$	$P 4_1 2_1 2$
a (Å)	6.9626	6.9706
b (Å)	6.9626	6.9706
c (Å)	19.5721	19.6915
A	90°	90°
В	90°	90°
γ	90°	90°
Cell Volume	948.08	956.79

as the absorption of UV and visible light includes the transition of electrons from  $\sigma$  and  $\pi$  orbitals in the ground state to higher energy states [22]. In this study, a UV–Visible SHIMADZU/UV-2600 series spectrometer was employed to record the transmission spectrum of both undoped and dye-doped GC single crystals within the range of 200 and 1100 nm. Single crystals are frequently employed in optical applications, making the transparency lower cut-off (200–400 nm) crucial for achieving second-harmonic generation (SHG) output with lasers. The material chosen for nonlinear optical (NLO) applications is required to possess this transparent quality within the visible range [23]. Fig. 4 illustrates the recorded optical transmittance spectrum of both undoped and dye-doped GC crystal.

The undoped GC crystal exhibited an absorption peak edge at 392 nm with 68% optical transparency in the visible wavelength range from 550 to 1100 nm. The peak at 392 nm typically corresponds to the absorption of light by molecules undergoing electronic transitions involving the  $\pi \to \pi^*$  transition of conjugated systems. This transition involves the excitation of electrons from the highest occupied molecular orbital (HOMO) to the lowest unoccupied molecular orbital (LUMO) within the conjugated system. The second peak at 508 nm also corresponds to the  $\pi \to \pi^*$  transition typically observed in molecules with extended  $\pi$  – conjugation, such as aromatic rings [24]. In contrast, the crystal doped with dye molecules displayed a blue-shifted absorption edge occurring at a shorter wavelength of 384 nm, with enhanced optical transparency of 74% due to the modification of the electronic structure from the incorporation of conjugated dye molecules. Upon doping, there is a notable change with the disappearance of the second peak at 508 nm in the dye-doped crystal compared to the undoped one. This could be attributed to the fact that when Pisolithus Arhizus dye molecules are incorporated into the GC crystal host matrix, they can effectively absorb light due to strong electronic transitions within the dye molecules. This efficient absorption by the dye molecules can led to the suppression or quenching of the host crystal's intrinsic absorption at the same wavelength, resulting in the disappearance of the 508 nm peak in the dye-doped spectrum. The UV-Visible spectrum indicates high transmittance within the range of 550-1100 nm for undoped GC and 400-1100 nm for dye-doped GC crystals, making them suitable choices for opto-electronic device fabrication and nonlinear optical (NLO) applications [25]. Dye doping not only decreases the structural grain boundaries within the crystal system but also enhances the optical quality of the GC crystal. The transparent window of both undoped and dye-doped GC crystals in the visible region facilitates effective optical transmission of the second harmonic frequencies of the Nd: YAG laser [26], indicating that the dye-doped GC crystals have enhanced transmittance compared to their undoped counterparts. The optical constant of a material plays a crucial role in fabricating optical devices as the dependence of the optical absorption coefficient on photon energy helps to determine the type of optical electron transitions that occur within the material [27]. When a dopant is intentionally introduced into the crystal structure, it can significantly modify the electronic structure and the

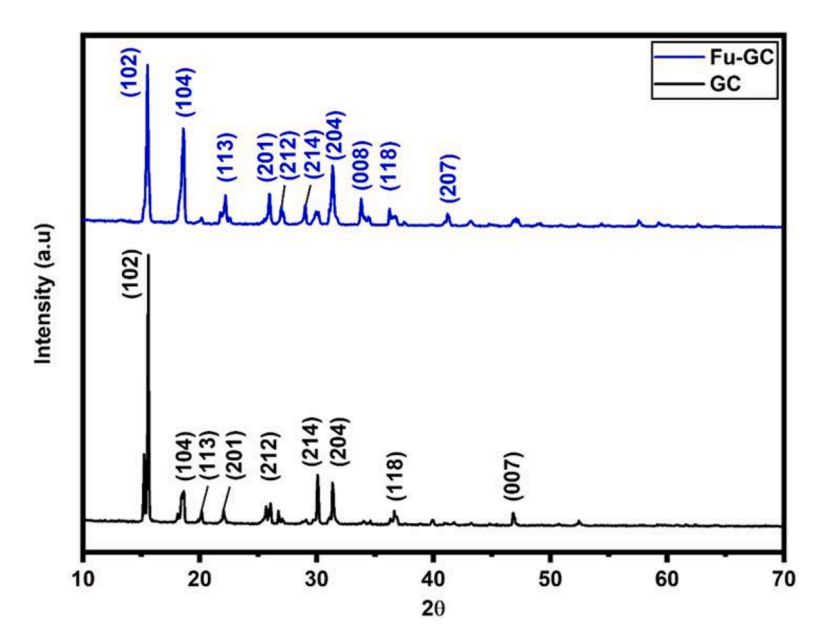


Fig. 3. Powder X-ray pattern for undoped and dye-doped GC crystals.

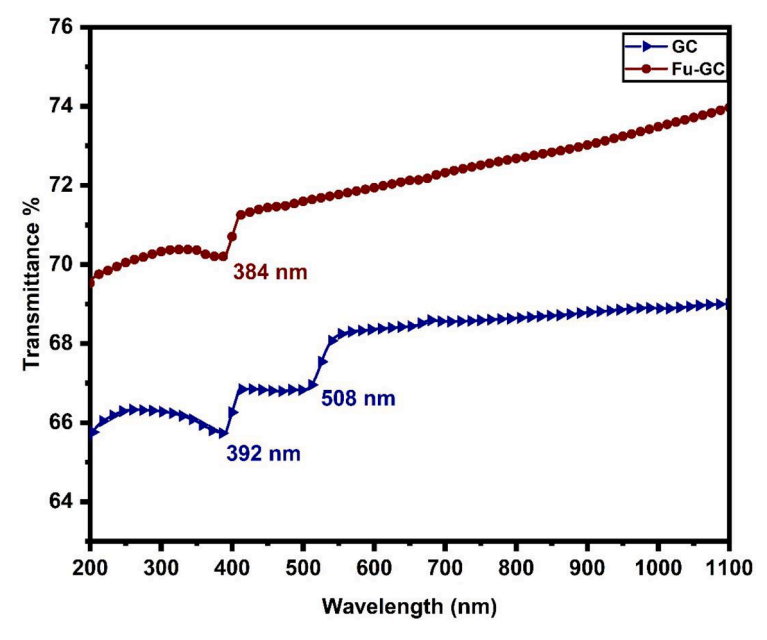


Fig. 4. UV-Visible transmittance spectrum of undoped and dye-doped GC crystals.

distribution of energy levels within the bandgap. The energy gap  $(E_g)$  is a fundamental parameter utilized to investigate the optical characteristics of a material.

Transmittance measurements were utilized to determine the absorption coefficient ( $\alpha$ ) using the relation [13]:

$$\alpha = \frac{2.302}{t} \log \left(\frac{1}{T}\right) \dots \tag{1}$$

where T is the transmittance and t is the thickness of the sample. In the high photon energy region, the energy-dependent behaviour of the absorption coefficient implies the presence of a direct bandgap in the crystals, as described by the following equation for high photon energies  $(h\nu)$  [28].

$$(\alpha h \nu)^2 = A \left( E_g - h \nu \right) \dots \tag{2}$$

where A is a constant,  $E_g$  is the optical bandgap, h is the Planck's constant and  $\nu$  is the frequency of the incident photons. The Tauc's graph depicting  $(\alpha h \nu)^2$  against the photon energy  $(h \nu)$  is illustrated in Fig. 5.

Thus, the bandgap of the crystals was determined by extending the linear portion of the graph to the energy axis, resulting in values of 2.67 eV for the undoped GC crystal and 3.28 eV for the dye-doped GC crystal. The aromatic  $\pi \to \pi^*$  transitions induced by the dye molecules widened the optical bandgap at the lower cut-off wavelength, although the transitions were localised within the dye molecules. Compared to the undoped crystal, dye-doped crystal exhibits a widened bandgap. This increase in the energy gap  $(E_g)$  can be attributed to factors associated with the incorporation of dye molecules into the crystal lattice. One of the factors is the modification of the electronic structure of the crystal due to the presence of dye molecules, leading to changes in the optical response of the material. This modification can alter the band structure of the crystal, leading to an increase in the optical bandgap.

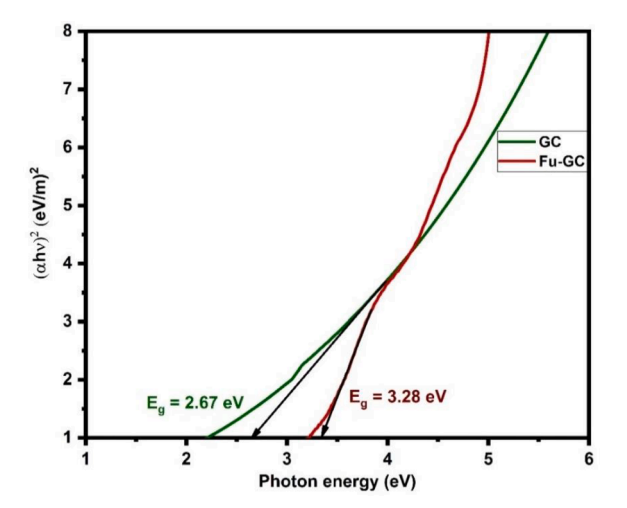


Fig. 5. Plots of  $(\alpha h \nu)^2$  function of  $(h \nu)$  with evaluation of bandgap of the material.

#### Photoluminescence (PL) analysis

Photoluminescence (PL) spectral analysis is an effective method that offers insights into the luminescence behaviour of the resulting optical materials [29]. The presence of imperfections plays a crucial role in influencing luminescent materials. Compounds characterized by an aromatic structure, long conjugated double bonds, and high resonance stability tend to exhibit luminescence. To achieve a strong photoluminescence, a higher-quality single crystals are needed [30]. The photoluminescence properties of both undoped and dye-doped GC single crystals were investigated using a SHIMADZU spectrofluorometer RF-5031 PC Series at ambient temperature. The powder samples of both undoped and dye-doped GC single crystals were excited at 400 nm and the resulting emission spectra were recorded. The observed spectrum is depicted in Figs. 6a and 6b.

The emission peak of the undoped GC crystal is centered at 563 nm, indicating green emission. A blue-shifted strong characteristic sharp emission peak appeared at 532 nm, indicating green emission, also noting a change in peak intensity in the dye-doped GC crystal. It is highlighted that no additional emission peaks were observed, indicating that the energy has been completely absorbed by the intermolecular ions. Thus, the crystals show great potential as a pure fluorescent material based on their luminescence in the solid form [31]. The high intensity of the photoluminescence emission indicates the low concentration of imperfections in the grown crystals, suggesting

potential applications in optical devices [27].

Fourier transform infrared (FTIR) spectroscopic analysis

In FTIR spectroscopy, infrared light is passed through a sample and the resulting infrared spectrum is recorded. The FTIR spectra provide information on the molecular structure, normal vibrational modes, bond types and bond strengths [32]. The FTIR spectra from 4000 to 400 cm<sup>-1</sup> were recorded on a PERKIN Elmer RX1 spectrometer using the KBr pellet technique. Fig. 7 displays mid-infrared transmission spectra of undoped and dye-doped guanidinium carbonate crystals, revealing a significant change in position and nature of the peaks.

This shift occurs because the doping of *Pisolithus Arhizus* dye in GC crystal typically results in changes to some characteristic vibrational frequencies and variations in peak intensities. The IR spectrum of the undoped GC crystal displayed an O—H stretching vibration band at 3371 cm<sup>-1</sup> and 3160 cm<sup>-1</sup> [33]. However, upon the incorporation of the *Pisolithus Arhizus* dye into the GC crystal matrix, the intensity of the peaks varies and there is a notable shift in peak position of these vibrations at 3386 and 3155 cm<sup>-1</sup> respectively, due to the influence of functional groups present in the dye molecules [34,35]. The vibrational modes associated with the stretching of the O—H bond are highly responsive and exhibit a broad range of variations in terms of intensity, bandwidth and wavenumber. These variations arise due to the influence of intra- or intermolecular hydrogen bonding interactions present within

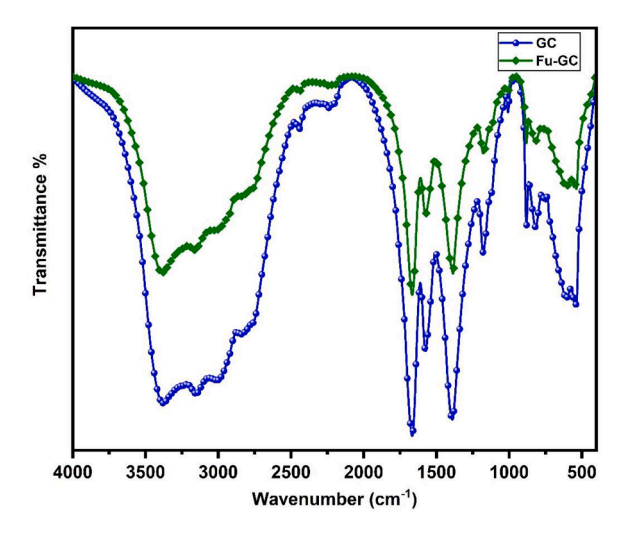
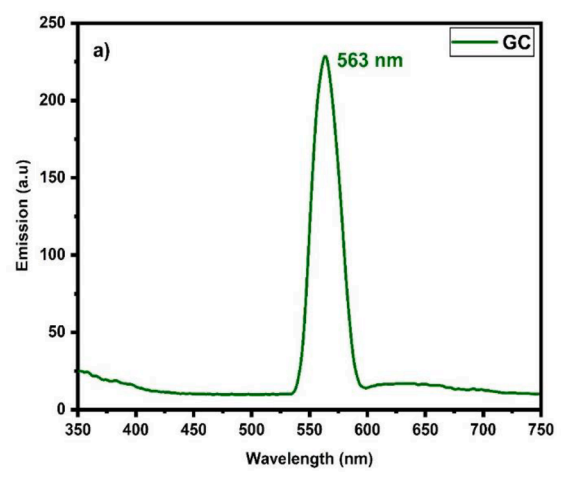


Fig. 7. FTIR spectrum of undoped and dye-doped GC single crystal.



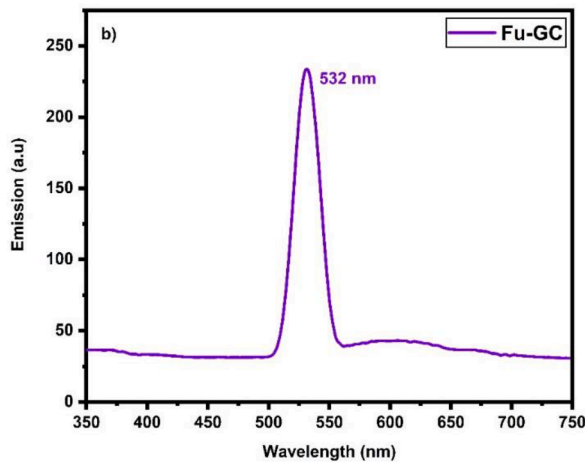


Fig. 6. a). Photoluminescence spectrum of undoped GC crystal b). Photoluminescence spectrum of dye-doped GC crystal.

the molecular structure [35]. The peaks at 3011 and 3013 cm $^{-1}$  are the N—H...O symmetric stretching vibrations of the nitrate group in undoped and dye-doped GC crystals respectively. This observation suggests an interaction between the N—H groups of guanidinium cations and the functional groups of the dye molecules dispersed within the crystal lattice. The undoped GC crystal shows an absorption peak at  $1670~{\rm cm}^{-1}$  which has been assigned to the in-plane bending vibration of the primary amine (-NH<sub>2</sub>) groups in the guanidinium cations [36]. Also, in the spectrum of dye-doped GC crystal, this vibration is shifted to a lower wavenumber appearing at  $1663~{\rm cm}^{-1}$ . This observation suggests that the incorporation of the fungal dye results in perturbation of the local environment of the amine functional groups, leading to changes in these vibrational modes of frequency.

The intense sharp peaks observed at 1571  $\mathrm{cm}^{-1}$  and 1579  $\mathrm{cm}^{-1}$ correspond to the stretching vibrations of the C = O moiety [37] for the undoped and dye-doped crystals, respectively. There is a slight shift in the peak position, and the intensity variation is due to the additional C = O bond vibrations present in the dye molecules. The peak at  $1383~\mathrm{cm}^{-1}$ is due to the aromatic ring vibrations of the C—H bond in the undoped crystals. In the dye-doped crystal, the peak intensity is strongly varied and the peak position is shifted to 1395 cm<sup>-1</sup> because of the C—H vibrations of the pulvinic acid that is present in the Pisolithus Arhizus fungus dye [19]. Both the undoped and dye-doped crystals exhibit an absorption peak at 1176 cm<sup>-1</sup> corresponding to the in-plane bending vibrations of the C-H bands associated with aromatic ring vibration. There is a variation in intensity is noticed for this peak between the two crystal samples, with the dye-doped crystals exhibiting a lower peak intensity relative to the undoped crystal. The presence of the peak at the same position indicates that the vibrational mode remains unchanged, while the intensity differences suggest the weakening of aromatic C-H bonds due to interactions with the dye molecules [33]. The undoped crystal displays an absorption band at 1007 cm<sup>-1</sup>, which can be assigned to the symmetric stretching vibration of the C—N bond [37]. Similarly in the dye-doped crystal, this C-N stretching peak undergoes a positive shift to 1012 cm<sup>-1</sup>. Additionally, the C—H out-of-plane bending modes occurs at 885 cm<sup>-1</sup> and 890 cm<sup>-1</sup> in the undoped and dye-doped crystals respectively [38].

The rocking vibration of the amine (NH $_2$ ) groups is observed at 605 cm $^{-1}$  for the undoped GC and 610 cm $^{-1}$  [36] for the dye-doped crystals as evidenced by corresponding peaks. The positive shift to higher wavenumbers for the NH $_2$  rocking mode in the dye molecules and amine functionalities of the crystal lattice indicates the effective integration. In general, the shift in peaks indicates the successful incorporation of the dye molecules in the crystal lattice. Table 2 lists the wavenumber assignments of undoped and dye-doped GC single crystals.

## Energy dispersive X-ray analysis (EDAX)

The energy dispersive X-ray analysis (EDAX) spectrum of both undoped and dye-doped GC crystals were recorded using a Carl ZEISS

**Table 2**FTIR vibrational modes of undoped and dye-doped GC crystals.

Wavenumber (cm <sup>-1</sup> )		Assignments	
Undoped GC	Fu-GC		
3371	3386	O-H Stretching vibration	
3160	3155	O—H Stretching vibration	
3011	3013	N-HO Symmetric stretching	
1670	1663	NH <sub>2</sub> in-plane bending	
1571	1579	Stretching vibrations of $C = O$	
1383	1395	Aromatic ring vibrations of C-H bond	
1176	1175	In-plane C—H bending vibration	
1007	1012	Symmetric C-N stretching vibration	
885	890	C-H out-of-plane bending vibration	
814	823	Out-of-plane bending vibration of nitrate	
605	610	Rocking mode of NH <sub>2</sub>	

EVO-18-Germany model with the X-ray range of 0–10 KeV. The EDAX spectrum and the elemental compositions of both samples are presented in Figs. 8 and 9.

The peaks observed in the 0–5 KeV range were emitted by X-rays as electrons returned to the K-electron shell (K $\alpha$ ). The EDAX spectrum of dye-doped crystal exhibits variation in the intensity of peaks and weight %, compared to the undoped crystal. Thus, the EDAX spectrum confirms the interaction of dye molecules with their undoped counterparts.

#### Thermogravimetric and differential thermal (TG-DTA) analysis

Thermogravimetric (TG) and differential thermal analysis (DTA) serve as valuable tool for obtaining insights into the decomposition temperature and phase transition of crystal systems. The TG-DTA analysis was performed using a Perkin Elmer STA-600 thermal analyzer in a nitrogen gas atmosphere with a heating rate of 20 °C/min, covering a temperature range from room temperature to 600 °C. Figs. 10 and 11 illustrates the TG-DTA spectra of GC crystals, highlighting both undoped and dye-doped samples. The analysis involved samples weighing 12.264 mg for the undoped and 10.762 mg for the dye-doped crystals.

The TG-DTA curve plots of both undoped and dve-doped GC crystals indicate their thermal stability. There is no observable weight loss up to 190 °C and 198 °C respectively. This clearly signifies the absence of moisture in both crystalline samples within these temperature ranges. For the undoped GC crystal, the first stage of weight loss is observed between 192 °C and 241 °C, with a major weight loss of 30%, which is attributed to the initiation of thermal decomposition of the crystal lattice or the release of volatile components. A second stage occurring in the temperature range from 241 °C to 340 °C, with a weight loss of 19%. In the case of dye-doped GC crystal (Fig. 11), the initial stage occurs between 200 °C and 246 °C, resulting in a significant weight loss of 26%, followed by a second stage extending from 246 °C to 349 °C, with a weight loss of 16%. After these weight losses, both materials were completely decomposed. Compared to undoped GC crystal the dyedoped GC crystal exhibits a slightly high thermal stability and there is an increase in the decomposition temperature.

A distinct endothermic peak at 225 °C in Fig. 10 is evident in the results of the differential thermal analysis (DTA) is associated with the melting point of an undoped GC crystal, while the peak at 230 °C in the undoped crystal, while, the peak at 230 °C in Fig. 11 for the dye-doped GC crystal signifies an initial phase of material decomposition above this temperature. Furthermore, a pronounced endothermic peak is observed at 338 °C in the DTA curve of the undoped crystal indicates the complete decomposition of the substance, aligning with the corresponding TG curve. Similarly, in the dye-doped crystal, the material starts to decompose at 345 °C. This improvement in thermal properties, attributed to the incorporation of dye molecules, into the crystal lattice. There is a notable change in thermal stability and decomposition temperature, the dye-doped crystal is suitable for the applications of up to 198 °C.

# Vickers' microhardness analysis

The mechanical properties such as hardness, yield strength and stiffness constant of the grown crystals were examined using a Vickers' microhardness test performed at room temperature. Different loads were applied using a Matsuzawa/VMT-X tester fitted with a diamond pyramidal indenter with an apex angle of 136 °C to analyze the samples. The three most important phenomena observed in the microhardness process are the anisotropy effect, the indentation size effect (ISE) and the reverse indentation size effect (RISE) [39]. The indentation size effect (ISE) refers to a decrease in hardness with increasing applied load whereas, the reverse indentation size effect (RISE) is characterized by an increase in hardness as the applied load increases. Hardness is strongly influenced by defects and intermolecular interactions, and it varies based on the degree of lattice order in the crystalline materials [40]. The Vickers' hardness number was calculated using the following relation:

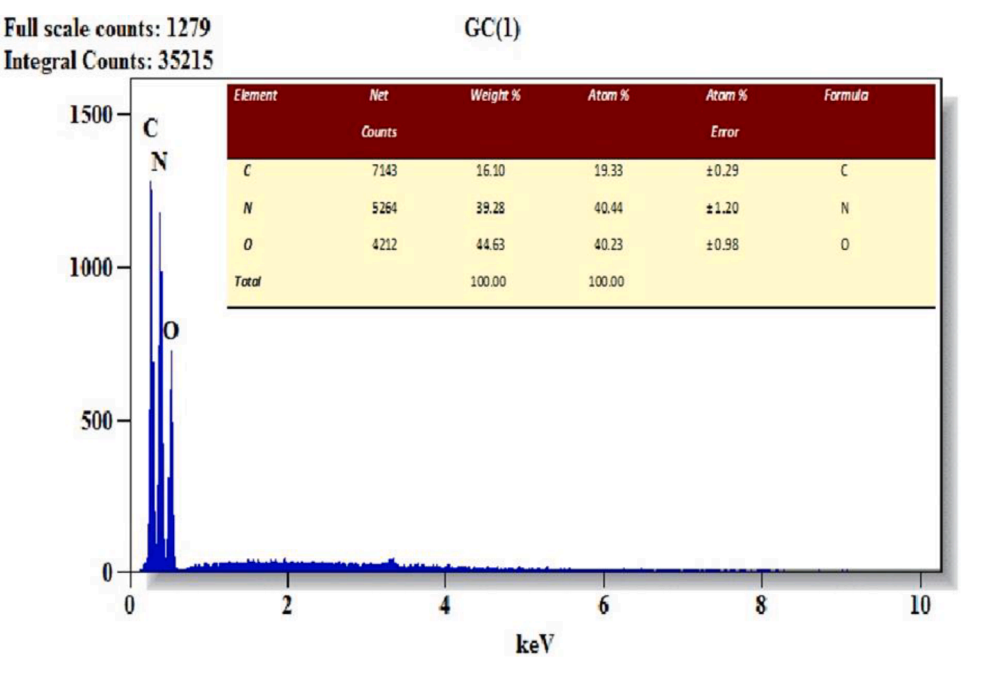


Fig. 8. EDAX spectrum of undoped GC single crystal.

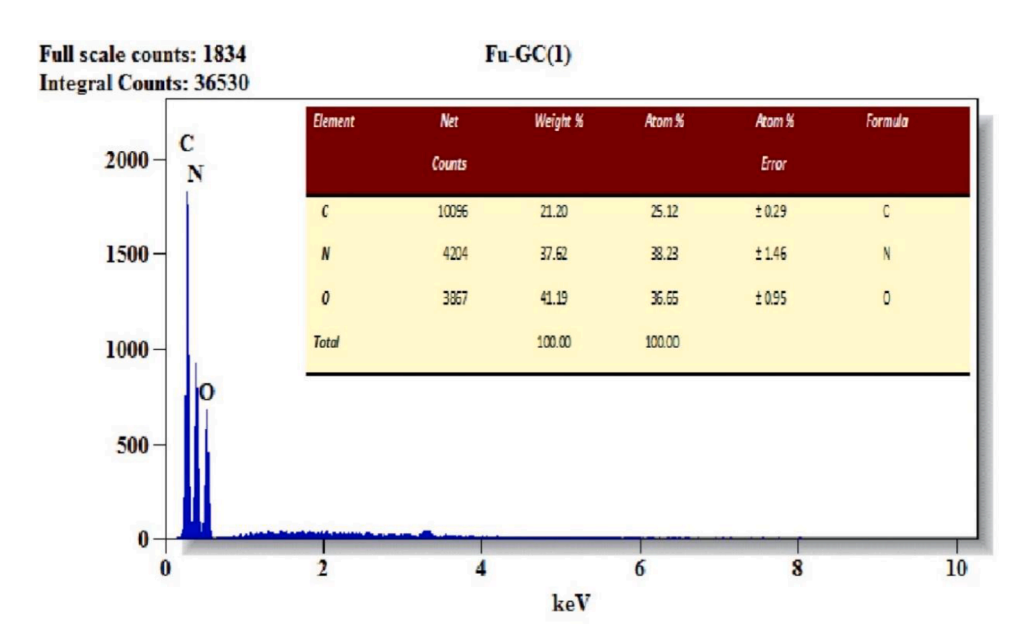


Fig. 9. EDAX spectrum of dye-doped GC single crystal.

$$H_V = \frac{KP}{d^2} \dots {3}$$

Where  $K = 2 Sin (136^{\circ} / 2)$ , P represents the indenter load and d denotes the average of two indentation diagonal lengths. Fig. 12 illustrates the variation in microhardness number with applied load for both undoped and dye-doped GC crystals. The materials' resistance to indenter penetration is assessed using the microhardness number  $(H_V)$ .

This value is notably influenced by the presence of inclusions, pores and cracks, thus offering crucial insights into the yield strength and tensile strengths of the grown crystals [41,42]. The Meyer's index number (n) of the crystals was calculated to analyze the nature of the grown crystals. Meyer's work hardening co-efficient (n) was determined by using Meyer's Power law [43]:

$$P = A d^n \dots (4)$$

Where A is a constant for a given material. According to Onitsch and Hanneman [44], the work hardening coefficient (n) ranged from 1 to 1.6 for hard materials, while for soft materials, it was greater than 1.6. The value of n was determined using the slope of the log P vs log d plot as illustrated in Fig. 13. The 'n' value for the undoped GC crystal is 1.70 and for the dye-doped GC, it is 1.65. Thus, both crystals fall into the soft material category. Cracks in the crystals become noticeable when the applied load exceeds 50 g. The decreased 'n' value in doped crystals indicates increased hardness due to dye doping.

Wooster's empirical equation [45] is used to obtain the elastic stiffness constant  $(C_{11})$  of the both undoped and dye-doped GC crystals.

$$C_{11} = (H_{\nu})^{(7/4)}...$$
 (5

The yield strength  $(\sigma_Y)$  of both crystal is calculated using the equation [46],

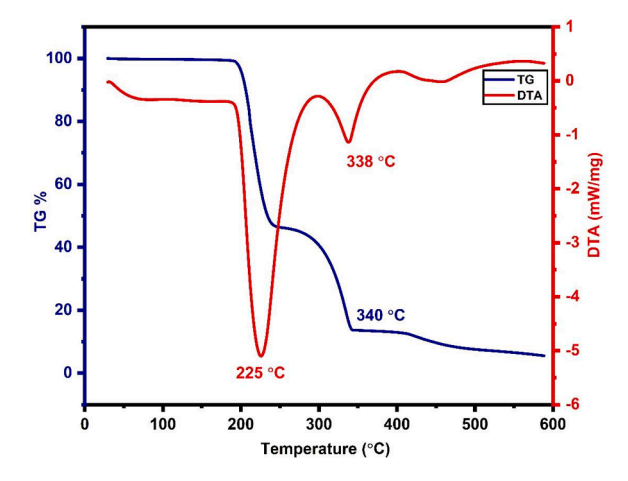


Fig. 10. TG-DTA curve of undoped GC crystal.

$$\sigma_{\rm Y} = \frac{H_{\rm v}}{3} \dots \tag{6}$$

Where  $H_{\nu}$  represents the microhardness of the material. Table 3 displays the calculated yield strength  $(\sigma_{Y})$  and elastic stiffness constant  $(C_{11})$  of both crystals under loads ranging from 2 to 50 g.

The results reveal that for both crystals, the yield strength and stiffness constant increase with an increase in applied load. The high values of yield strength and stiffness constant indicate strong bonding between atoms in the crystal lattices, making these materials suitable for use in NLO devices.

#### Second harmonic generation (SHG) analysis

The Kurtz-Perry powder analysis was employed to measure the nonlinear optical (NLO) property of the grown crystals. A Q-switched Nd: YAG laser with a pulse width of 6 ns and a fundamental wavelength of 1064 nm was applied to the sample. The emission of green radiation at 532 nm from both crystalline samples confirmed the presence of nonlinear optical properties in the grown crystals. A digital oscilloscope was used to display the second harmonic generation (SHG) efficiency output signal, which was then converted into an electrical signal. The incident optical signal was detected by a photomultiplier tube and transformed into an output voltage. The second harmonic signal of 14.9

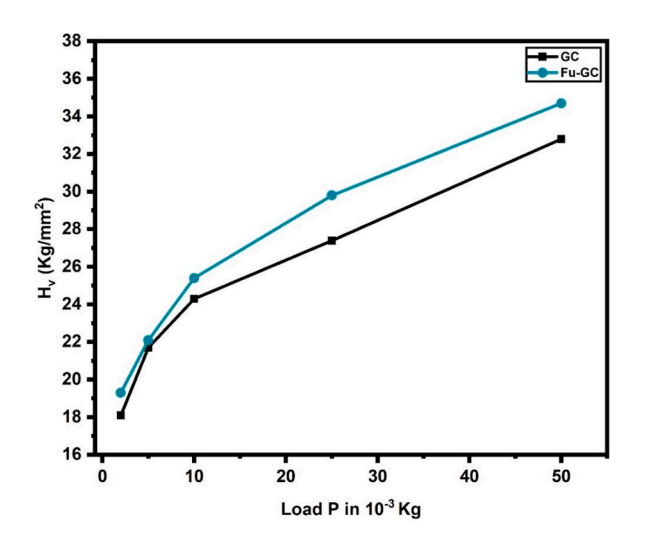


**Fig. 12.** Variation of Hardness  $H_{\nu}$  with load P.

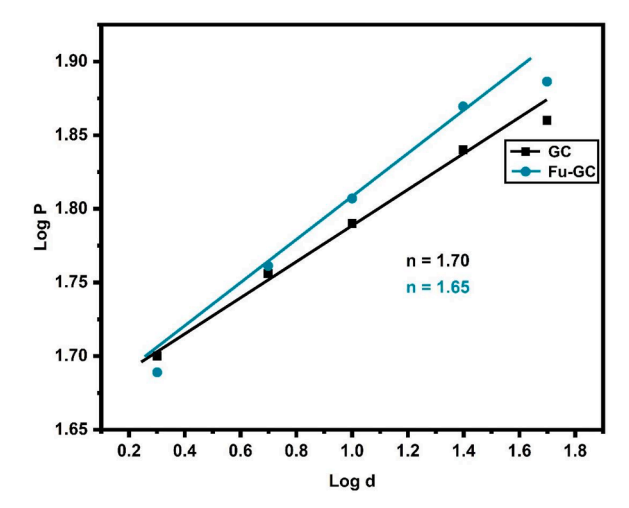


Fig. 13. A plot of log P vs log d for both undoped and dye-doped crystals.

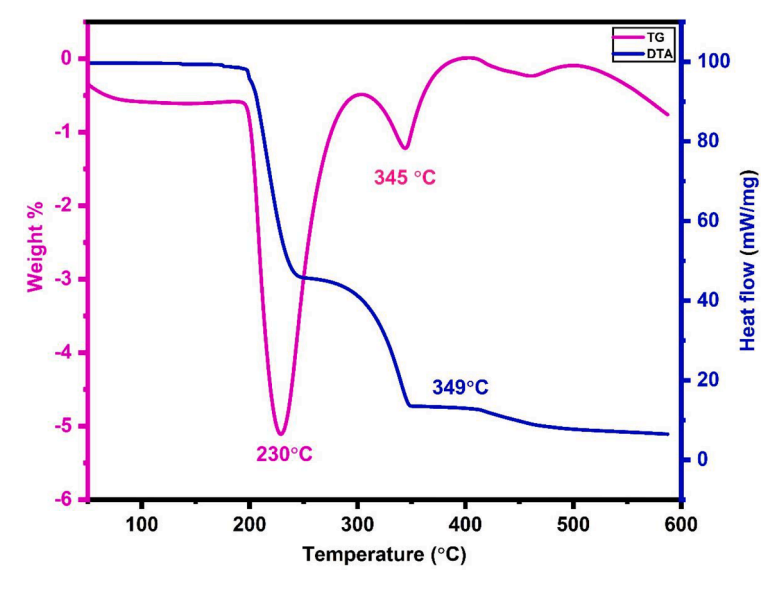


Fig. 11. TG-DTA curve of dye-doped GC crystal.

Table 3 Stiffness Constant  $(C_{11})$  and yield strength  $(\sigma_Y)$  of both undoped and dye-doped crystals.

Samples	Load (P)	$C_{11} \times 10^{14} \text{ N/m}^2$	$\sigma_Y \times 10^6 \text{ N/m}^2$
Undoped GC Crystal	2	6.03	158.83
	5	7.23	218.17
	10	8.10	265.95
	25	9.13	328.14
	50	10.94	449.15
Dye-doped GC Crystal	2	6.43	177.71
	5	7.36	225.38
	10	8.48	287.38
	25	9.92	380.08
	50	11.57	496.10

mV was obtained for the pure GC powder crystal sample with an input energy of  $0.70 \, \text{mJ/Pulse}$ . For the dye-doped powder GC crystal sample, a signal of  $25.8 \, \text{mV}$  was obtained whereas the standard potassium dihydrogen phosphate (KDP) reference sample yielded a SHG signal of  $7.5 \, \text{mV}$  for the same input energy.

The second harmonic generation (SHG) efficiency of undoped GC crystal is 1.98 times and dye-doped GC crystal exhibits 3.44 times higher efficiency than that of the standard KDP material. Based on these results, the SHG effective nonlinearity of dye-doped GC is 1.73 times that of undoped GC. Consequently, dye-doped crystals are preferrable for nonlinear optical device applications compared to undoped GC crystals.

#### Conclusion

High-quality single crystals of both undoped and naturally Pisolithus Arhizus dye-doped guanidinium carbonate were successfully grown using the slow evaporation method. Single crystal and powder X-ray diffraction analysis confirmed the crystalline nature of both undoped and dye-doped crystals. UV-Visible analysis revealed that the dye-doped crystals exhibit excellent optical transparency (74%), compared to the pure ones (68%). Photoluminescence studies demonstrated emission properties in both crystals at their respective wavelengths. FTIR and EDAX analyses confirmed the presence of dye molecules in the crystal lattice. Enhanced thermal stability was observed in the dye-doped crystals, making them suitable for potential applications up to 198 °C. Dye-doped GC crystals were found to be mechanically more stable than pure GC crystals. The second harmonic generation efficiency of the undoped GC crystals is 1.98 times while the dye-doped GC crystals has an efficiency of 3.44 times greater than that of KDP. The dye-doped crystals exhibit large second-order nonlinear optical co-efficient, making them promising candidates for various nonlinear optical applications such as second-harmonic generation, optical switching and electrooptic modulation. However, it is important to consider potential limitations associated with the use of fungal dye dopants in nonlinear optical applications, such as sourcing, sustainability and long-term stability, as well as potential environmental impact of using natural dye sources. Continued research into these aspects will further elucidate the practical viability and sustainability of Pisolithus Arhizus dye-doped guanidinium carbonate crystals in various applications. Overall, in comparison to the undoped guanidinium carbonate single crystals, the Pisolithus Arhizus natural dve-doped guanidinium carbonate single crystals exhibit a large second-order nonlinear efficiency, making them a promising candidate for various nonlinear optical applications such as second-harmonic generation, optical switching and electro-optic modulation.

#### CRediT authorship contribution statement

K. Divya: Writing – original draft, Validation, Methodology, Investigation, Data curation. Amutha Soosairaj: Visualization, Formal analysis. A. Alex Arunmozhi: Formal analysis, Visualization. A. Leo Rajesh: Conceptualization, Resources, Supervision, Validation.

#### **Declaration of competing interest**

The authors declare that they have no known competing financial interests or personal relationships that could have appeared to influence the work reported in this paper.

#### Data availability

The data are included in the manuscript in the form of figures and tables.

#### References

- [1] B.Milton Boaz, A.L. Rajesh, S.X.J. Raja, S.J. Das, Growth and characterization of a new nonlinear optical semiorganic lithium paranitrophenolate trihydrate (NO2-C6H 4-OLi-3H2O) single crystal, J. Cryst. Growth. 262 (2004) 531–535, https:// doi.org/10.1016/j.jcrysgro.2003.10.041.
- [2] A. Ponchitra, K. Balasubramanian, R. Jothi Mani, K. Sakthipandi, Structural, mechanical, dielectric, thermal, and nonlinear optical properties of zinc-doped ninhydrin single crystals, Indian J. Phys. 96 (2022) 2313–2321, https://doi.org/ 10.1007/s12648-021-02163-5.
- [3] K. Divya, A. Soosairaj, D.P. Pabba, V.S. Manikandan, A. Thirumurugan, Ethanol assisted synthesis and characterization of semiorganic lithium para nitrophenolate dihydrate single crystals, J. Mater. Sci. Mater. Electron. (2024) 1–9, https://doi.org/10.1007/s10854-024-12331-y.
- [4] P. Era, R.M. Jauhar, T. Kamalesh, T. Prakash, V. Siva, Theoretical insight on the optical centred electrical properties of guanidinium isophthalate NLO crystal for electro-optic Q switches, Heliyon 9 (2023), https://doi.org/10.1016/j. heliyon.2023.e18311 e18311.
- [5] A. Arputhalatha, M. Anbuchezhiyan, G. Palani, Synthesis, growth, physio-chemical and Hirshfeld surface analysis of guanidinium l-glutamate single crystal, J. Mater. Sci. Mater. Electron. 32 (2021) 12503–12512, https://doi.org/10.1007/s10854-021-05884-9.
- [6] T. Arumanayagam, P. Murugakoothan, Growth, linear and nonlinear optical studies on guanidinium 4-nitrobenzoate (GuNB): An organic NLO material, Optik (Stuttg) 123 (2012) 1153–1156, https://doi.org/10.1016/j.ijleo.2011.05.037.
- [7] T. Arumanayagam, P. Murugakoothan, Studies on optical and mechanical properties of new organic NLO crystal: Guanidinium 4-aminobenzoate (GuAB), Mater. Lett. 65 (2011) 2748–2750, https://doi.org/10.1016/j.matlet.2011.05.081.
- [8] M.P. Nancy, J.M. Linet, Synthesis, growth, structural, thermal, mechanical and optical properties of barium guanidinium dichloride (BaGuCl2) single crystal for NLO applications, J. Opt. 49 (2020) 351–356, https://doi.org/10.1007/s12596-020-00625-3.
- [9] G.R. Desiraju, G.W. Parshall, Crystal engineering: the design of organic solids, Mater. Sci. Monogr. 54 (1989).
- [10] M. Dhavamurthy, G. Peramaiyan, S.S.S. Babu, R. Mohan, Synthesis, growth and characterization studies of p-hydroxybenzoic acid addition with the guanidinium carbonate single-crystals, J. Mol. Eng. Mater. 02 (2014) 1450006, https://doi.org/ 10.1142/s2251237314500063.
- [11] P. Vivek, G.S. Kumar, A. Steephen, R.M. Jauhar, A. Suvitha, M. Rekha, M. Kowsalya, N. Karunagaran, R. Arunkumar, Development of organic crystalline nature guanidinium nitrate (GuN): structural, frontier molecular orbital, optical, thermal, mechanical, theoretical and experimental SHG and Z-scan properties for NLO device uses, J. Mater. Sci. Mater. Electron. 32 (2021) 4493–4504, https://doi. org/10.1007/s10854-020-05190-w.
- [12] M.K. Dhatchaiyini, G. Rajasekar, M. NizamMohideen, A. Bhaskaran, Investigation on structural, spectral, optical, thermal studies and third order NLO properties of guanidinium pentaborate monohydrate single crystal, J. Mol. Struct. 1210 (2020) 128065, https://doi.org/10.1016/j.molstruc.2020.128065.
- [13] P. Era, R.M. Jauhar, P. Murugakoothan, Optimization of growth parameters and investigations on the physico-chemical properties of an organometallic guanidinium chromate single crystal for nonlinear optical and optical limiting applications, Opt. Mater. (Amst). 99 (2020) 109558, https://doi.org/10.1016/j. optmat.2019.109558.
- [14] G. Chaithra, P.R. Deepthi, W. Sultana, M. Challa, A. Sukhdev, P.M. Kumar, B. C. Hemaraju, J. Shanthi, Exploring the influence of safranin dye on optical, thermal and dielectric properties of TGA crystal for SSDL applications, J. Mater. Sci. Mater. Electron. 34 (2023) 29. https://doi.org/10.1007/s10854-022-09466-1.
- [15] J.H. Joshi, S. Kalainathan, D.K. Kanchan, K. Chaudhari, M.J. Joshi, K.D. Parikh, Crystal growth, structural, optical, photoluminescence, electrical and third-order nonlinear optical studies of pure and methylene blue dye-doped ammonium dihydrogen phosphate crystals, J. Mater. Sci. Mater. Electron. 34 (2023) 21, https://doi.org/10.1007/s10854-022-09447-4.
- [16] P. Mohammed Yusuf Ansari, R.M. Muthukrishnan, R. Imran Khan, C. Vedhi, K. Sakthipandi, S.M. Abdul Kader, Green synthesis of copper oxide nanoparticles using Amaranthus dubius leaf extract for sensor and photocatalytic applications, Chem. Phys. Impact. 7 (2023) 100374, https://doi.org/10.1016/j. chpbi.2023.100374.
- [17] M. Mirjalili, L. Karimi, Extraction and characterization of natural dye from green walnut shells and its use in dyeing polyamide: Focus on antibacterial properties, J. Chem. (2013), 2013.

- [18] N.K. Naik, R. Naika, GC-MS analysis of Pisolithus arrhizus (Scop.) Rauschert, (1959), a non-edible wild mushroom in search of novel bioactive compounds collected from Western Ghats of Karnataka, India, Int. J. Bot. Stud. 6 (2021) 204–209. www.botanyjournals.com.
- [19] A.G.N. Camara, F.W.Q. Almeida-Neto, Y.L.C. Silva, F.M. Nunes, M.C. Mattos, J. Mafezoli, F.G. Barbosa, E.S. Marinho, P. Lima-Neto, M.C.F. Oliveira, IR and UV-VIS spectroscopic characterization of norbadione A and study of the electronic properties of other pigments derived from pulvinic acid, J. Mol. Struct. 1285 (2023) 135491, https://doi.org/10.1016/j.molstruc.2023.135491.
- [20] M. Gill, M. Kiefel, Pigments of Fungi. XXXVII. Pisoquinone, a New Naphthalenoid Pulvinic Acid From the Fungus Pisolithus arhizus, Aust. J. Chem. 47 (1967), https://doi.org/10.1071/ch9941967, 1994.
- [21] J.M. Adams, R.W.H. Small, The crystal structure of guanidinium carbonate, Acta Crystallogr. Sect. B Struct. Crystallogr. Cryst. Chem. 30 (1974) 2191–2193, https://doi.org/10.1107/s0567740874006716.
- [22] S. Masilamani, A.M. Musthafa, Chemical analysis, FTIR and microhardness study to find out nonlinear optical property of 1-asparagine lithium chloride: A semiorganic crystal, Microchem. J. 110 (2013) 749–752, https://doi.org/10.1016/j. microc. 2013.09.003
- [23] P.R. Kumar, R. Gunaseelan, S. Kumararaman, G. Baghavannarayana, P. Sagayaraj, Unidirectional growth, structural, optical and mechanical properties of LTA crystal, Mater. Chem. Phys. 125 (2011) 15–19, https://doi.org/10.1016/j. matchemphys.2010.07.036.
- [24] L.D.S. Yadav, Ultraviolet and Visible, Org. Spectrosc. (2005) 7-51.
- [25] S. Dinakaran, S. Verma, S.J. Das, Solubility, crystal growth, morphology, crystalline perfection and optical homogeneity of lithium p-nitrophenolate trihydrate, a semiorganic NLO crystal, CrystEngComm 13 (2011) 2375–2380, https://doi.org/10.1039/c0ce00663g.
- [26] K. Krishnaraj, N. Sivakumar, P.P. Kumar, Growth, spectral, mechanical, electrical and optical characterization of guanidinium hydrogen succinate single crystal, Bull. Mater. Sci. (2020) 43, https://doi.org/10.1007/s12034-019-2019-6.
- [27] J. Dalal, N. Sinha, H. Yadav, B. Kumar, Structural, electrical, ferroelectric and mechanical properties with Hirshfeld surface analysis of novel NLO semiorganic sodium p-nitrophenolate dihydrate piezoelectric single crystal, RSC Adv 5 (2015) 57735–57748, https://doi.org/10.1039/c5ra10501c.
- [28] J.C. Tauc, Semiconductor Amorphous and Liquid (1974) 195.
- [29] M. Saravanan, Growth and characterization of dexterous nonlinear optical material: Dimethyl amino pyridinium 4-nitrophenolate 4-nitrophenol (DMAPNP), Opt. Mater. (Amst). 58 (2016) 327–341, https://doi.org/10.1016/j. optmat.2016.06.002.
- [30] T. Kanagasekaran, P. Mythili, P. Srinivasan, A.Y. Nooraldeen, P.K. Palanisamy, R. Gopalakrishnan, Studies on the growth, optical, thermal, and mechanical properties of pure and o-nitroaniline doped benzil crystals, Cryst. Growth Des. 8 (2008) 2335–2339, https://doi.org/10.1021/cg701132f.
- [31] M. Dhavamurthy, G. Peramaiyan, M. Nizam Mohideen, S. Kalainathan, R. Mohan, Structural, growth and optical characterizations of an organic third-order nonlinear crystal: Guanidinium trichloroacetate, J. Nonlinear Opt. Phys. Mater. 24 (2015) 1–14, https://doi.org/10.1142/S0218863515500459.

- [32] B. Smith, Infrared spectral interpretation: A systematic approach, Infrared Spectr. Interpret. A Syst. Approach. (2018) 1–304, https://doi.org/10.1201/ 9780203750841
- [33] K. Nakamoto, Infrared and Raman spectra of Inorganic and Coordination compounds, Part B: Applications in coordination, organometallic, and Bioinorganic Chemistry, John Wiley & Sons, 2009.
- [34] N. Mani, D. Nicksonsebastin, M. Prasath, Quantum computational, spectroscopic, ADMET, molecular docking and dynamics simulation revealing the inhibition of psoralidin against anti-tuberculosis, Chem. Phys. Impact. 7 (2023) 100292, https://doi.org/10.1016/j.chphi.2023.100292.
- [35] S. Bangaru, G. Madhu, M. Srinivasan, P. Manivannan, Exploring flexibility, intermolecular interactions and ADMET profiles of anti-influenza agent isorhapontigenin: A quantum chemical and molecular docking study, Heliyon 8 (2022), https://doi.org/10.1016/j.heliyon.2022.e10122.
- [36] A. Suvitha, P. Murugakoothan, Synthesis, growth, structural, spectroscopic and optical studies of a semiorganic NLO crystal: Zinc guanidinium phosphate, Spectrochim. Acta - Part A Mol. Biomol. Spectrosc. 86 (2012) 266–270, https://doi.org/10.1016/j.saa.2011.10.034.
- [37] T. Arumanayagam, S. Ananth, P. Murugakoothan, Studies on growth, spectral, optical and mechanical properties of new organic NLO crystal: Guanidinium l-glutamate (GuGL), Spectrochim. Acta Part A Mol. Biomol. Spectrosc. 97 (2012) 741–745, https://doi.org/10.1016/j.saa.2012.07.039.
- [38] G. Saravana Kumar, P. Murugakoothan, Synthesis, spectral analysis, optical and thermal properties of new organic NLO crystal: N,N'-Diphenylguanidinium Nitrate (DPGN), Spectrochim. Acta - Part A Mol. Biomol. Spectrosc. 131 (2014) 17–21, https://doi.org/10.1016/j.saa.2014.04.059.
- [39] O. Sahin, O. Uzun, U. Kolemen, N. Ucar, Vickers microindentation hardness studies of β-Sn single crystals, Mater. Charact. 58 (2007) 197–204, https://doi.org/ 10.1016/j.matchar.2006.04.023.
- [40] K.K. Bamzai, P.N. Kotru, Fracture Mechanics, Crack Propagation and Microhardness Studies on Flux Grown ErAlO\_3 Single Crystals, 材料科学技术 英文版 (2000) 405–410.
- [41] N. Tyagi, N. Sinha, H. Yadav, B. Kumar, Pyroelectric properties and conduction mechanism in solution grown glycine sodium nitrate single crystal, Phys. B Condens. Matter. 462 (2015) 18–24, https://doi.org/10.1016/j. physb.2015.01.005.
- [42] H. Yadav, N. Sinha, N. Tyagi, B. Kumar, Enhancement of optical, piezoelectric, and mechanical properties in crystal violet dye-doped benzophenone crystals grown by Czochralski technique, Cryst. Growth Des. 15 (2015) 4908–4917, https://doi.org/ 10.1021/acs.cgd.5b00792.
- [43] N. Sinha, S. Bhandari, H. Yadav, G. Ray, S. Godara, N. Tyagi, J. Dalal, S. Kumar, B. Kumar, Performance of crystal violet doped triglycine sulfate single crystals for optical and communication applications, CrystEngComm 17 (2015) 5757–5767, https://doi.org/10.1039/c5ce00703h.
- [44] E.M. ONITSCH, [Systematic metallographic and mineralogic structures], Mikroskopie 5 (1950) 94–96.
- [45] W.A. Wooster, Physical properties and atomic arrangements in crystals, Reports Prog. Phys. 16 (1953) 62–82, https://doi.org/10.1088/0034-4885/16/1/302.
- [46] D. Roylance, Mechanical properties of materials, (2008).